Spectroscopic Evidence for Exceptional Thermal Contribution to Electron Beam-Induced Fragmentation

Marissa A. Caldwell,[†] Ben Haynor,[‡] Shaul Aloni,[‡] D. Frank Ogletree,[‡] H.-S. Philip Wong,[†] Jeffrey J. Urban,*[,‡] and Delia J. Milliron*[,‡]

Departments of Chemistry and Electrical Engineering and Center for Integrated Systems, Stanford University, Stanford, California 94305, United States, and The Molecular Foundry, Lawrence Berkeley National Laboratory, Berkeley, California 94720, United States

While electron beam-induced fragmentation (EBIF) has been reported to result in the formation of nanocrystals of various compositions, the physical forces driving this phenomenon are still poorly understood. We report EBIF to be a much more general phenomenon than previously appreciated, operative across a wide variety of metals, semiconductors, and insulators. In addition, we leverage the temperature dependent bandgap of several semiconductors, using in situ cathodoluminescence spectroscopy, to quantify the thermal contribution to EBIF and find extreme temperature rises upward of 1000 K.

Introduction

Recent advances in electron microscopy have enabled new insights into the structural, electronic, and optical properties of matter at nanometer and subnanometer length scales. This includes the detailed characterization of static nanomaterials and, increasingly, the dynamic structure and properties of nanomaterials subject to external perturbations. For instance, in situ electron microscopy has recently made possible the atomic to nanometer scale observation of thermally induced structural changes of Pt nanoparticles,[1] semiconductor nanowire[2,3] and carbon nanotube growth processes,[4] and the dynamic structure of catalytic copper nanoparticles exposed to carbon monoxide.[5] While remarkably useful probes of nanoscale structure, electron-beam microscopies involve bombardment of samples with highly energetic beams of electrons. Unsurprisingly, this can induce changes in the material under investigation, an observation that has been successfully leveraged as a fabrication and patterning tool in selected instances, as in e-beam lithography,[6] the direct fabrication of metal nanostructures,[7] and inorganic nanocrystal formation by electron-beam induced fragmentation (EBIF).[8−14]

EBIF is a general term for the phenomenon in which nanocrystals are formed by irradiating a larger (usually micrometer-sized) piece of material with a high-energy electron beam, such as one typically found in a scanning electron microscope (SEM) or transmission electron microscope (TEM). Previously, several individual materials have been reported to demonstrate EBIF, including Au,[8] Pb,[9] BiNi,[10,14] SnO_2,[11] and GeTe,[12] and metal particles have been formed from the corresponding azides.[13] In all cases, the same empirical observations have been reported; upon irradiation with a sufficiently high energy electron beam, a larger particle of source material shrinks simultaneously with the formation of a field of smaller nanocrystals (generally of the same or similar composition) of varying sizes. The nanocrystals nearest to the original source particle are the largest, while the smallest nanocrystals are found the furthest away. Here, we investigate the generality of EBIF by exposing micrometer-sized pieces of a wide variety of materials to electron beam irradiation. We additionally employ cathodoluminescence spectroscopy (CL) to quantify the thermal contribution to EBIF phenomena.

Experimental Section

To achieve micrometer-sized particles, commercially available bulk materials were ground using a mortar and pestle. The fine powders were suspended in toluene and dropped onto a carbon support film spanning a copper TEM grid (400 mesh) and allowed to dry. GaN microwires were grown in a Thomas Swan CCS reactor on c-plane sapphire substrates in a nitrogen atmosphere. Nickel films 1 nm thick were used as catalysts. The wires were grown at 850 °C and 100 Torr for 10 min from trimethylgallium (125 μmol/min) and NH_3 (25 mmol/min). Following the synthesis, the wires were dry transferred to a lacy carbon support film spanning a copper grid. The samples were loaded into the TEM or SEM for EBIF and spectroscopic investigations.

CL measurements were performed in a Zeiss Supra 55VP SEM with beam current controlled by changing the aperture selection and current mode. With the beam in spot mode, luminescence was collected using a 250 μm UV−vis optical fiber (Ocean Optics) coupled to a QE6500 Ocean Optics CCD spectrometer for spectroscopy or a quartz waveguide coupled to R6094 Hamamatsu photomultiplier tube for CL imaging. TEM of GaN microwires was performed on an analytical JEOL 2100-F. Other materials were imaged using a TOPCON 002b; both TEMs were operated at $V_{acc} = 200$ kV. To induce EBIF, a micrometer scale particle was exposed to a condensed electron beam at crossover for a few seconds before the beam was returned to normal imaging conditions. Beam current was controlled by changing the condenser aperture size. The resulting nanoparticles were imaged under standard conditions. Some materials showed instability under normal imaging conditions and required much lower beam current for imaging.

Results and Discussion

To assess the generality of EBIF, we surveyed a number of different materials, spanning a wide range of physical, electronic,

* To whom correspondence should be addressed. E-mail: (J.J.U.) jjurban@lbl.gov; (D.J.M.) dmilliron@lbl.gov.
[†] Stanford University.
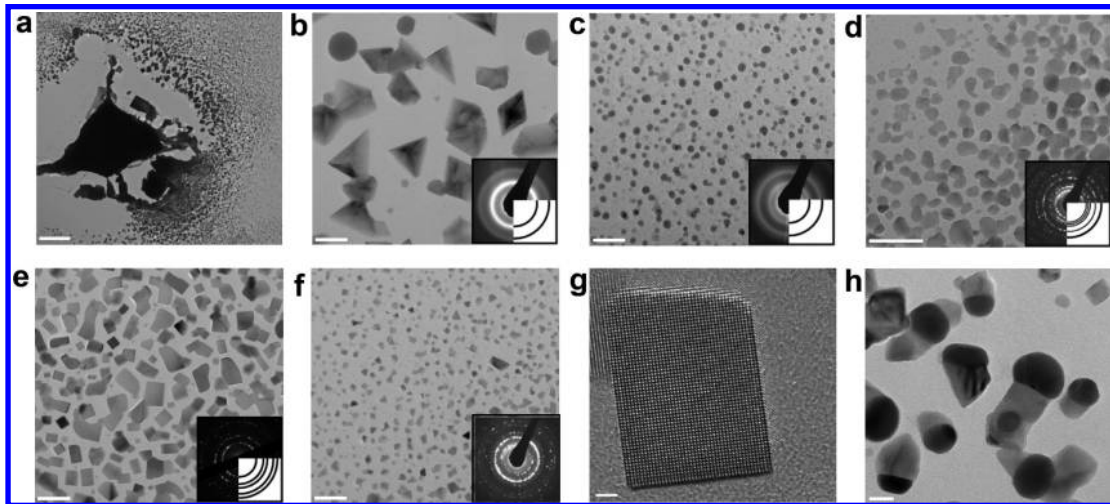[‡] Lawrence Berkeley National Laboratory.

Figure 1. Transmission electron microscopy images of inorganic nanomaterials formed by beam-induced vaporization. (a) Low-magnification image showing source material and surrounding PbTe nanocrystals (scale bar = 1 μm). (b–g) Sb, Ge, ZnO, PbSe, Ge–Sb–Te nanocrystals (scale bars = 40 nm) and PbSe (high resolution, scale bar = 2 nm), respectively, with electron diffraction patterns shown as insets, where digital matches to the JCPDS patterns are illustrated in the lower right. (h) Early phase growth of GeTe nanowires seeded from colloidal Au nanoparticles (scale bar = 20 nm).

TABLE 1: Material Compositions Demonstrating EBIF

type	materials
metals	Se, Sb, Te, Ge, Te, LuAl$_3$, YbAl$_3$, CeCoIn$_5$, Au[b], Bi–Ni[b], Cu[b], Ag[b]
semiconductors	PbTe, PbS, PbSe, Bi$_2$Te$_3$, Bi$_2$Se$_3$, In$_2$Se$_3$, GeSe, GeTe[a], Sb$_2$Te$_3$, Ge$_2$Sb$_2$Te$_5$, Ge$_{15}$Sb$_{85}$, CdS, CdSe, CdTe, SnTe, ZnSe, GaN wires
insulators	ZnO, Ta$_2$O$_5$, SnO[b], PbO[b]

[a] Denotes material previously reported and investigated in this publication. [b] Denotes materials previously reported in the literature and not demonstrated in this publication.

and chemical properties. Nearly all materials investigated demonstrated EBIF to some degree (Figure 1, Table 1) with the only exception being GeSe$_2$. Qualitatively, certain materials fragmented very readily, while other materials required careful control over the beam condensation rate or location of the source material relative to the Cu grid. In the case of the lanthanide-containing materials, the larger pieces were often repelled by the electron beam, but still fragmented when they could be trapped by either another piece or the carbon so the beam could be condensed onto them. Additionally, by collocating gold nanoparticles next to source material, heterogeneous growth of extended GeTe structures was observed (Figure 1h).

The fact that semiconductors readily fragment provided an opportunity to quantify the thermal energies induced by the electron beam. While it has been established that an electron beam can interact with the specimen through multiple pathways including[15] e-beam sputtering, radiolysis, electrostatic disruption, hot electron relaxation, and knock-on damage, several authors have postulated that the material must go through the melt during EBIF.[8–10,13] Simple thermal models of electron beam-material interactions predict that beam-induced heating is strongly dependent on thermal conductivity and should only become significant for good insulators.[16,17] The extent of local heating has been commonly modeled by assuming that energy locally deposited by the beam is conducted away laterally through the specimen. This model assumes a specimen film whose edges contact a thermal sink, fixing a boundary condition of zero temperature rise. For good thermal insulators, with $\kappa = 0.1$ W/m-K, 100 K or more local temperature rise can be anticipated under imaging conditions, but moderately higher thermal con-

ductivities ($\kappa = 1$–10 W/m-K) reduce this estimate to tens of degrees. Under this model, metals ($\kappa = 100$–400 W/m-K) do not measurably heat up; in fact, thin metal coatings can be used to prevent heating of delicate specimens. A few careful experiments have directly measured temperature changes adjacent to an incident electron beam, improving accuracy of temperature rise estimates.[18–20] However, the qualitative assessment remains that thermally conductive materials will not heat up under imaging conditions and only excellent insulators such as polymers can become locally very hot.

To resolve the apparent contradiction between the expectation of material-specific beam-induced heating effects and the observed material generality of EBIF, we employed CL to measure the local temperature of the material being irradiated by the electron beam. When a semiconductor is illuminated by an electron beam, a small fraction of the incoming electrons create electron–hole pairs which can then recombine, emitting a photon with the characteristic energy of the bandgap. Because semiconductor bandgaps predictably shift to lower energy with increasing temperature, the resulting band gap CL spectrum reflects the local temperature.[21] However, the peak emission energy of a semiconductor can be significantly shifted by electronic as well as thermal effects.[22] The CL spectrum of a piece of CdS in thermal contact with copper ($\kappa = 400$ W/m-K) was collected to prevent heating and isolate beam-induced electric field effects. The peak position, and any field-induced shift, was found to be independent of beam current (Figure 2a) and it agrees well with that reported by Achour for CL of thick films of CdS at low beam currents.[18] In addition, only a slight shift in peak position at high beam power was observed for particles resting on a 50 nm thick Si$_3$N$_4$ film on a silicon wafer ($\kappa = 150$ W/m-K) (Supplementary Figure 1). Si$_3$N$_4$, unlike copper, is a good electrical insulator yet still provides a reasonable heat sink ($\kappa \sim 30$ W/m-K), so this result confirms the lack of a beam power-dependent field-induced peak shift. Turning to particles of CdS suspended on the carbon support film, the peak position is only slightly shifted at low beam currents, indicating negligible heating. However, the spectra of these particles, unlike those on thermally conductive copper or Si$_3$N$_4$, shift significantly with increasing beam power (Figure 2b). This shift reflects the extent of beam-induced heating.

Spectroscopic Evidence for Thermal Contribution to EBIF

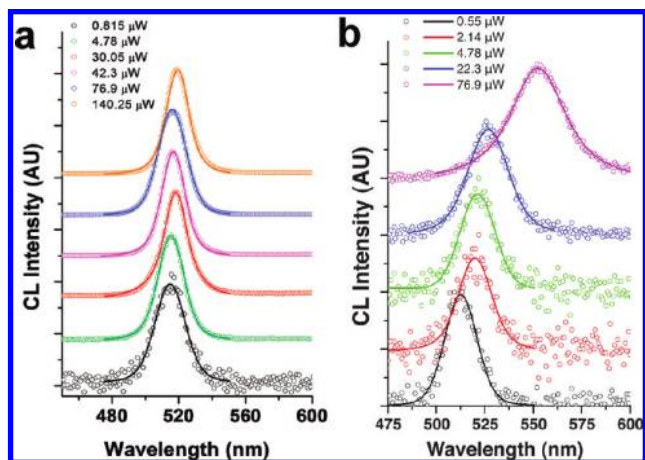*J. Phys. Chem. C, Vol. xxx, No. xx, XXXX* **C**

Figure 2. Cathodoluminescence (CL) spectra of micrometer-sized pieces of CdS over a range of incident beam currents (a) supported by Cu and (b) supported on ultrathin carbon. Lines are fits of Voigt functions to the data.

Using the known temperature dependence of the CdS bandgap, the local lattice temperature can be derived from the CL peak position and followed as a function of beam current. The temperature dependence of semiconductor bandgaps have been described by a number of semiempirical and theoretical models. The Varshni relation[23] is the most basic semiempirical model that fits experimental data, but it has little theoretical basis. On the other hand, purely theoretical models do not reproduce experimental data, especially in the low-temperature regime.[24] We derive temperature changes using the model proposed by O'Donnell and Chen[25] that fits experimental data better than the Varshni relation and includes physically meaningful fitting parameters. The model is $E_g(T) = E_g(0) - S\langle h\omega \rangle [\coth(\langle h\omega \rangle/2kT) - 1]$ where $E_g(0)$ is a fitting parameter related to the bandgap at 0 K, S is a dimensionless coupling constant, the Huang–Rhys parameter, and $\langle h\omega \rangle$ is the average phonon energy. At high temperatures, $kT \gg \langle h\omega \rangle$, the expression simplifies into a linear form: $E_g(T) = E_g(0) - 2SkT$, implying that the degree of electron–phonon coupling, not the average phonon energy, determines the decrease in bandgap at high temperatures. For hexagonal CdS and CdSe, the fitting parameters are known.[26] The CL spectra are fit with Voigt functions to determine peak positions, these peak values are compared to those at low beam current, and then the O'Donnell and Chen equation is used to derive the temperature change. The resulting temperatures, reached in the range of conventional imaging conditions, can exceed 1000 K (Figure 3).

To investigate the mechanism of such substantial heating, temperature changes are measured at various beam accelerating voltages (V_{acc}). Increasing V_{acc} increases the penetration depth of the beam since inelastic scattering scales inversely with electron energy.[27] In silicon, for example, 5 kV electrons are expected to penetrate ~100 nm whereas 15 kV electrons will sample over a micrometer of the material. However, local temperature was found to depend only on the overall power (IV_{acc}) of the beam within the precision of the measurement (Figure 3a), indicating that the entire micrometer-sized piece of source material is approximately isothermal. This is consistent with an estimated 1.4 K temperature gradient across a micrometer-sized particle of CdSe (see Supporting Information). The conventional models used to estimate predicted specimen heating[16,17] (discussed above) assume that such effective conduction provides a pathway to a thermal sink, preventing significant local thermal loads. This is, however, not the case
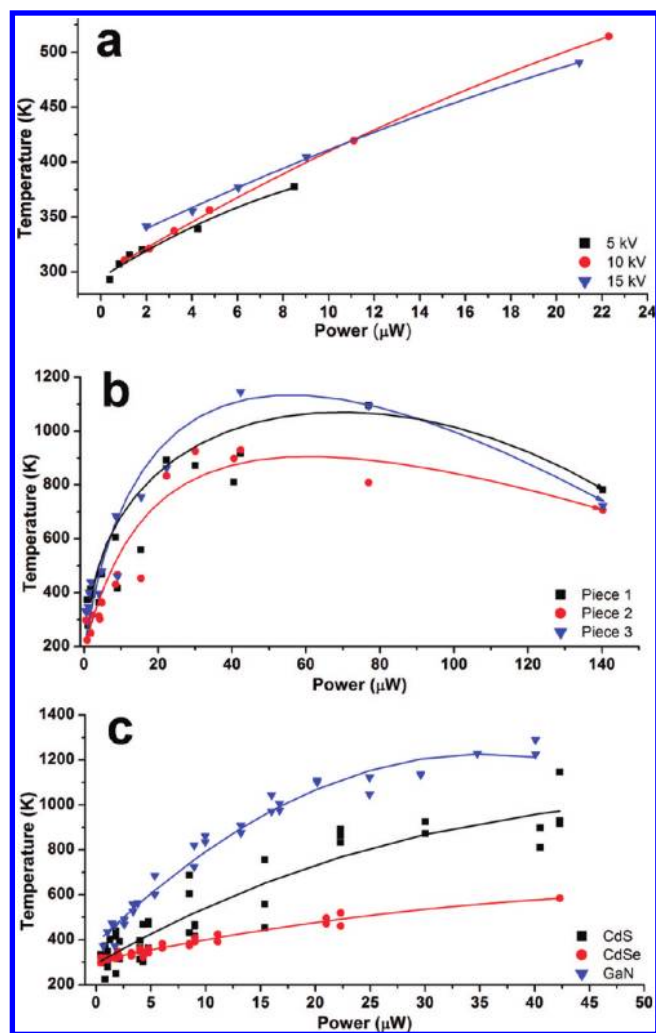

Figure 3. (a) Local temperature of CdS derived from CL spectra as a function of electron beam power at various accelerating voltage. (b) Derived temperature of three distinct micrometer scale pieces of CdS as a function of beam power. (c) Comparison of derived temperature of GaN, CdS, and CdSe as a function of beam power. Data from three pieces of CdS, two pieces of CdSe, and two GaN microwires are plotted together. In all cases, the derived temperature rise was added to 293 K (approximate ambient temperature) to give the approximate absolute temperature. Lines are guides to the eye.

for a specimen suspended on a thin carbon support film that forms a thermal bottleneck and allows the remarkable degree of local heating observed in our measurements. The dependence on power, rather than V_{acc}, suggests why obvious sample damage is not generally observed under standard imaging conditions. In an SEM, under normal imaging conditions, $V_{acc} \sim 5$ kV, and the resultant beam power is typically less than 10 μW. This is below the power needed for very extreme heating and the associated potential for serious damage but still sufficient to induce 100 K or more thermal loads. Irradiation in a TEM, where $V_{acc} \sim 200$ kV, can easily reach the high beam powers at which even more significant heating was observed, which may significantly influence processes such as semiconductor nanowire growth[2] being observed in situ in a TEM, for example.

To control for the effects of crystalline structure and grain boundaries on the temperature rises, single crystalline GaN microwires were subjected to electron beam irradiation. These wires are well suited for this experiment as they both (1) possess intense band-edge luminescence that facilitates single-microwire CL studies and (2) are of an intermediate size that allows lattice-
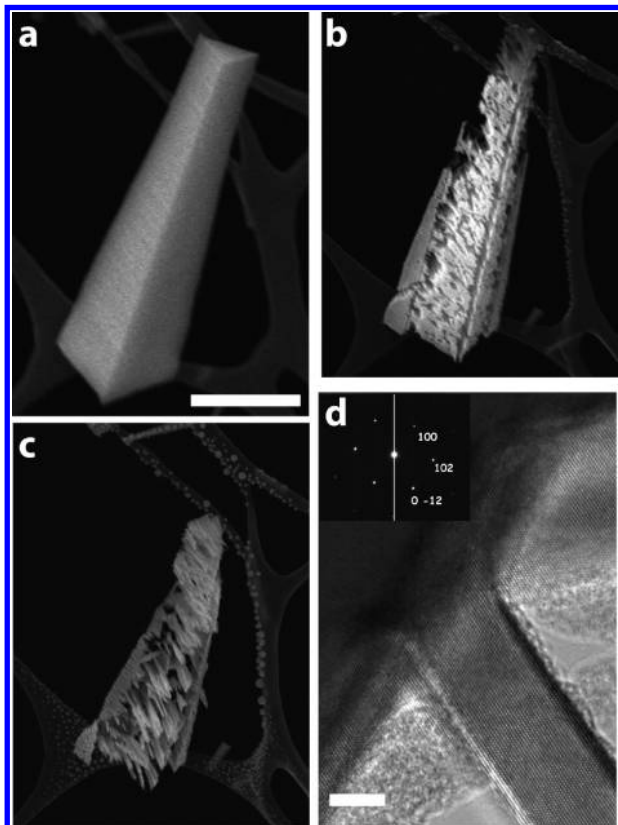
Figure 4. (a−c) SEM showing the progressive material loss from a GaN microwire under focused electron beam irradiation. Scale bar is 2 μm. (a) Before the onset of illumination (b) after a brief illumination (c) after full illumination. (d) High-resolution TEM on one of the branches and diffraction (inset) after illumination. Scale bar is 5 nm.

resolved imaging in the TEM while still possessing sufficient volume to have a large interaction cross-section with the beam. All wires studied are single-crystalline, single-phase, wurtzite GaN wires of triangular cross-section grown from the vapor phase along the [2 1 0] direction with well-defined side facets. Their band edge luminescence falls at E_g ~3.39 eV at 300 K and they behave (in terms of thermal, dielectric, and vibrational properties) as a "bulk" semiconductor.

Upon irradiation in an electron beam, the microwires exhibit characteristic EBIF behavior in which the original wire loses significant material with the simultaneous formation of small nanoparticles on the surrounding substrate (Figure 4). Notably, a significant difference was observed in the remaining source material. Generally in EBIF, the source material decomposes in an uncontrolled fashion; the GaN microwires, however, begin to decompose at high energy edge sites (comprised of N atoms) and continue with pitting and directional erosion perpendicular to the long axis of the microwire. This leads to a characteristic "comb" morphology (Figure 4b,c). Examination of the "teeth" of the comb by high-resolution transmission electron microscopy (HRTEM) and electron diffraction, indicates that the long axis of the "teeth" lie along the [0 0 2] direction, perpendicular to the long axis of the original microwire (Figure 4d). These observations are consistent with the damage process being initiated by loss of N (as N_2) followed by further material loss, eroding the microwire in such a way that high energy polar surfaces (002 and 00$\bar{2}$) are eliminated in favor of nonpolar surface terminations.

Above a vaporization threshold of ~1500 K, GaN is known to decompose by loss of N_2 to the gas phase,[28] consistent

with the hypothesis that the microwires are suffering from extreme beam-induced heating effects during EBIF. To determine if it is plausible that the wires are reaching high enough temperatures for vaporization, the CL spectra of wires were collected under different electron beam conditions. For wires in contact with the copper mesh, only a small shift of the CL peak was observed, reflecting a small current-dependent electronic effect on the spectrum. In comparison, a wire suspended on a lacey carbon support film exhibited a peak position that depended strongly upon beam current, similar to CdS and CdSe (Supporting Information Figure 2). In the case of GaN, the O'Donnell and Chen parameters were extracted from previously published data[29] and used to determine the local temperature of the wire. The resulting temperatures, measured below the threshold for obvious material loss, exceed 1200 K (Figure 3c), consistent with the EBIF damage pathway being thermally driven.

For each material, the CL-derived temperatures vary little between unique micrometer-sized pieces (Figure 3b, Supporting Information Figure 2b), making the extent of local heating a reproducible function of electron beam power. As a result, meaningful comparisons of beam heating can be made between different materials, including data collected on multiple pieces of each. Electron irradiation produced local temperatures that decreased in the order GaN > CdS > CdSe across a wide range of beam powers (Figure 3c). This qualitative trend must arise from differences in the balance between beam-induced heating and heat dissipation by convection, conduction, and radiation. Convective and radiative cooling are each insignificant in the vacuum environment of the microscope (see Supporting Information). Thus, thermal conduction is the dominant heat dissipation pathway. However, the greater thermal conductivity of single crystalline GaN (κ = 130 W/m-K)[30] versus CdS (κ = 16 W/m-K)[31] versus CdSe (κ = 6.9 W/m-K)[31] predicts a temperature trend opposite that which is observed. To understand this discrepancy, we must consider highly nonequilibrium heat transfer, which has been modeled in the context of pulsed laser ablation of metals and semiconductors.[32] Local temperature rises are dominated by electron−phonon coupling, which transfers energy from the electron beam to the semiconductor lattice. In this case, the higher values of electron−phonon coupling constants (S = 2.81 for GaN,[33,34] 2.16 for CdS, 1.67 for CdSe[35]) and Debye temperatures (θ_D = 600K for GaN,[30] 219 K for CdS,[31] and 181 K for CdSe[31]) correlate with more efficient thermal excitation of GaN than CdS than CdSe. While differences in efficiency of thermal excitation are consistent with our findings, contributions by differences in crystalline quality and interfacial thermal conductivity cannot conclusively be dismissed. However, standard theoretical treatments of thermal transport across boundaries predict the converse temperature rises for these three materials (see Supporting Information). Thus, the high temperatures measured by CL result from efficient coupling of energy from scattered electrons into phonons and limited heat conduction away from the micrometer-scale source materials, leading to a large thermal contribution to EBIF.

Conclusion

In conclusion, EBIF is shown to be a much more general phenomenon than previously reported in the literature with materials from metals to semiconductors to insulators exhibiting the phenomenon. The inclusion of semiconductors on the list of materials demonstrating EBIF allows for the quantification of the local temperature rises through CL spectroscopy. Local

Spectroscopic Evidence for Thermal Contribution to EBIF

J. Phys. Chem. C, Vol. xxx, No. xx, XXXX **E**

temperatures rise dramatically for all semiconductors investigated, exceeding 1000 K for both CdS micrometer-scale pieces and single crystalline GaN microwires, with the degree of heating correlated with the extent of electron−phonon coupling. These high temperatures point to a significant thermal contribution to EBIF, consistent with earlier hypotheses that EBIF occurs by a mechanism in which the materials go through a thermally induced phase transition. The universality of e-beam-induced heating can be leveraged to prepare nanocrystals of materials that are otherwise difficult to synthesize by chemical routes. Nanocrystals down to a few nanometers are readily formed in preference to continuous films with immediate feedback using the imaging and spectroscopic capabilities of the electron microscope. Utilizing this feedback loop, EBIF can be readily controlled by adjusting the beam current and voltage and can be leveraged as a general method for production of nanocrystals in pursuit of size-dependent properties.

Supporting Information Available: Scanning electron microscopy image and additional CL data for CdS, as well as CL data for GaN microwires and analysis of these by the model discussed in the text. Additional discussion of thermal conductance effects related to the experiments described. This material is available free of charge via the Internet at http://pubs.acs.org.

References and Notes

(1) Wang, Z. L.; Petroski, J. M.; Green, T. C.; El-Sayed, M. A. *J. Phys. Chem. B* **1998**, *102*, 6145–6151.

(2) Kodambaka, S.; Tersoff, J.; Reuter, M. C.; Ross, F. M. *Science* **2007**, *316*, 729–732.

(3) Hofmann, S.; Sharma, R.; Wirth, C. T.; Cervantes-Sodi, F.; Ducati, C.; Kasama, T.; Dunin-Borkowski, R. E.; Drucker, J.; Bennett, P.; Robertson, J. *Nat. Mater.* **2008**, *7*, 372–375.

(4) Hofmann, S.; Sharma, R.; Ducati, C.; Du, G.; Mattevi, C.; Cepek, C.; Cantoro, M.; Pisana, S.; Parvez, A.; Cervantes-Sodi, F.; Ferrari, A. C.; Dunin-Borkowski, R.; Lizzit, S.; Petaccia, L.; Goldoni, A.; Robertson, J. *Nano Lett.* **2007**, *7*, 602–608.

(5) Hansen, P. L.; Wagner, J. B.; Helveg, S.; Rostrup-Nielsen, J. R.; Clausen, B. S.; Topsoe, H. *Science* **2002**, *295*, 2053–2055.

(6) McCord, M. A.; Rooks, M. J. *Handbook of Microlithography, Micromachining and Microfabrication: Microlithography*; Rai-Choudhury, P., Ed.; Institution of Engineering and Technology: Hertfordshire, U.K., 1997; Vol. 1.

(7) Fischbein, M. D.; Drndic, M. *Nano Lett.* **2007**, *7*, 1329–1337.

(8) Ru, Q. *Appl. Phys. Lett.* **1997**, *71*, 1792–1794.

(9) Pan, Z. W.; Dai, Z. R.; Wang, Z. L. *Appl. Phys. Lett.* **2002**, *80*, 309–311.

(10) Pyrz, W. D.; Park, S.; Blom, D. A.; Buttrey, D. J.; Vogt, T. *J. Phys. Chem. C* **2010**, *114*, 2538–2543.

(11) Lu, B.; Wang, C.; Zhang, Y. *Appl. Phys. Lett.* **1997**, *70*, 717–719.

(12) Buck, M. R.; Sines, I. T.; Schaak, R. E. *Chem. Mater.* **2010**, *22*, 3236–3240.

(13) Herley, P. J.; Jones, W. *Z. Phys. D: At., Mol., Clusters* **1993**, *26*, 159–161.

(14) Pyrz, W. D.; Park, S.; Vogt, T.; Buttrey, D. J. *J. Phys. Chem. C* **2007**, *111*, 10824–10828.

(15) Wang, Z. L. *J. Phys. Chem. B* **2000**, *104*, 1153–1175.

(16) Egerton, R. F.; Li, P.; Malac, M. *Micron* **2004**, *35*, 399–409.

(17) Hobbs, L. W. In *Introduction to Analytical Electron Microscopy*; Hren, J. J., Goldstein, J. I., Joy, D. C., Ed.; Plenum Press: New York, 1979.

(18) Achour, S. *Philos. Mag. B* **1990**, *62*, 329–336.

(19) Gatos, C. H.; Vaughan, J. J.; Lagowski, J.; Gatos, H. C. *J. Appl. Phys.* **1981**, *52*, 1464–1469.

(20) Lee, K.; Myers, T. H. *J. Electron. Mater.* **2007**, *36*, 431–435.

(21) Petrov, V. I. *Phys. Status Solidi A* **1992**, *133*, 189–230.

(22) Yacobi, B. G. *Phys. Rev. B* **1980**, *22*, 1007.

(23) Varshni, Y. P. *Physica* **1967**, *34*, 149–154.

(24) Lautenschlager, P.; Allen, P. B.; Cardona, M. *Phys. Rev. B* **1985**, *31*, 2163.

(25) O'Donnell, K. P.; Chen, X. *Appl. Phys. Lett.* **1991**, *58*, 2924–2926.

(26) O'Donnell, K. P., Middleton, P. G. In *Properties of Wide Bandgap II-VI Semiconductors*; Bhargava, R., Ed.; INSPEC: London, 1997.

(27) Bieringer, R. J. *Phys. Rev.* **1966**, *142*, 550.

(28) Iijima, S.; Ichihashi, T. *Phys. Rev. Lett.* **1986**, *56*, 616.

(29) Passler, R.; Griebl, E.; Riepl, H.; Lautner, G.; Bauer, S.; Preis, H.; Gebhardt, W.; Buda, B.; As, D. J.; Schikora, D.; Lischka, K.; Papagelis, K.; Ves, S. *J. Appl. Phys.* **1999**, *86*, 4403–4411.

(30) *Properties, Processing and Applications of Gallium Nitride and Related Semiconductors*; Edgar, J. H., Strite, S., Akasaki, I., Amano, H., Wetzel, C., Ed.; INSPEC: London, 1999.

(31) Madelung, O.; Rosslet, U.; Schulz, M. *Landolt-Bornstein-Group III Condensed Matter: II-VI and I-VIII Compounds; Semimagnetic Compounds*; Springer-Verlag: Germany, 1999.

(32) Lin, Z.; Zhigilei, L. V. *Appl. Surf. Sci.* **2007**, *253*, 6295–6300.

(33) Germain, M.; Kartheuser, E.; Gurskii, A. L.; Lutsenko, E. V.; Marko, I. P.; Pavlovskii, V. N.; Yablonskii, G. P.; Heime, K.; Heuken, M.; Schineller, B. *J. Appl. Phys.* **2002**, *91*, 9827–9834.

(34) We report a conservative value of $S = 2.81$ here. There is tremendous dispersion in reported literature values of the Huang−Rhys parameter for GaN (ranging from 0.76 to 5.1, for similar techniques). Analysis of S in this material is complicated deeply by well-known defect state luminescence and complicated valence band structure, two factors that are not present in either CdS or CdSe. Empirical support for this value comes from the knowledge that GaN is unusually polar relative to other II-VI semiconductors (as judged by values of the piezoelectric coefficients and LO phonon energies).

(35) Ungier, W.; Suffczynski, M.; Adamowski, J. *Phys. Rev. B* **1981**, *24*, 2109.